Lawrence Berkeley National Laboratory

Lawrence Berkeley National Laboratory

Title

Lithographic performance evaluation of a contaminated EUV mask after cleaning

Permalink

https://escholarship.org/uc/item/4sm1d0cs

Author

George, Simi

Publication Date

2010-01-31

Peer reviewed

eScholarship.org Powered by the California Digital Library
University of California

Lithographic performance evaluation of a contaminated EUV mask after cleaning

Running title: Lithographic performance evaluation of contaminated EUV mask

Running Authors: George, Naulleau, Okoroanyanwu, Dittmar, Holfeld, and Wüest

Simi George[a)] and Patrick Naulleau

Center for X-ray Optics, Lawrence Berkeley National Laboratory, 1 Cyclotron Road, Berkeley, CA, 94720

Uzodinma Okoroanyanwu

GlobalFoundries, 257 Fuller Road, Albany, NY 12203

Kornelia Dittmar

GlobalFoundries, Wilschdorfer Landstr. 101, 01109 Dresden, Germany

Christian Holfeld

Advanced Mask Technology Center GmbH & Co. KG, Rähnitzer Allee 9, 01109 Dresden, Germany

Andrea Wüest

SEMATECH, 257 Fuller Road, Albany, NY 12203

[a)]Electronic Mail: sageorge@lbl.gov

The effect of surface contamination and subsequent mask surface cleaning on the lithographic performance of a EUV mask is investigated. SEMATECH's Berkeley micro-field exposure tool (MET) printed 40 nm and 50 nm line and space (L/S) patterns are evaluated to compare the performance of a contaminated and cleaned mask to an uncontaminated mask. Since the two EUV masks have distinct absorber architectures, optical imaging models and aerial image calculations were completed to determine any expected differences in performance. Measured and calculated Bossung curves, process windows, and exposure latitudes for the two sets of L/S patterns are compared to determine how the contamination and cleaning impacts the lithographic performance of EUV masks. The observed differences in mask performance are shown to be insignificant, indicating that the cleaning process did not appreciably affect mask performance.

I. Introduction

Reflective extreme ultraviolet (EUV) lithography[1, 2, 3, 4] masks[5, 6] present new challenges in pattern transfer to the wafer. Contamination of the EUV reticle due to various surface

deposition processes results in the loss of image contrast and exposure latitude in patterning[7, 8]. Achieving workable mask lifetimes, consequently, requires the contaminated masks to be cleaned[9]. The viability of the mask cleaning process requires the cleaning to have a negligible impact on imaging performance when compared to a pristine mask.

To study the viability of a cleaning process, we used the SEMATECH Berkeley micro-field exposure tool (MET) to compare the imaging performance of a contaminated and subsequently cleaned EUV mask to a fresh mask. A fresh mask was used for comparison because comparable exposure data on the original mask before contamination was not available. The fresh mask is comprised of a different absorber stack potentially leading to some uncertainty in the comparison. To address this concern, rigorous electromagnetic simulations were performed to directly compare the two different mask architectures.

II. Contamination and Cleaning

A. Mask Absorber Architecture

The basic structure of EUV masks start with a substrate of low thermal expansion with 40 or more layer pairs of Mo-Si deposited on top for providing high EUV reflectivity. A capping layer is sputtered on top of the multilayer pairs and lithographic patterning is completed with a buffer/absorber stack over all of the mirror layers. The contaminated mask that was cleaned, subsequently referred to as the *test* mask, had a 70 nm Chromium absorber layer while the *reference* mask structure had a 55 nm TaBN absorber on top of a 15 nm TaON anti-reflection coating (ARC) layer. Additionally, the masks have different bias conditions applied to the absorber pattern. The details of the two mask structures and the corresponding material properties at 13.5 nm (92 eV) used for the simulations are in Table 1 and Table 2

Table 1: **Contaminated/Cleaned TAR70 EUV mask (*test* mask)**
Table 2: **Uncontaminated LR-TaBN reference EUV mask (*reference* mask)**

B. Procedure Description

Before cleaning, the *test* mask was used in the SEMATECH Berkeley MET for resist testing. After approximately two years of use and having suffered significant reflectivity loss, the

test mask was removed from the system and sent to Global Foundries and to the Advanced Mask Technology Center (AMTC) to be analyzed and cleaned.

Analysis of the contamination was performed with scanning electron microscopy (SEM) and auger electron spectroscopy (AES). The SEM was a ZEISS Ultra 55 high resolution tool with thermal field emission source. The images were taken from top down at a voltage of 5 kV. The AES equipment was the Physical Electronics PHI Smart 200 tool, which was equipped with a field emission electron source, cylindrical mirror analyzer (CMA), and Argon sputter ion gun. The measurements were carried out at a primary electron beam voltage of 10 kV, whereas the Carbon mapping of the exposed and contaminated area was carried out at 1kV to get the appropriate field of view.

After analyzing the contamination, the mask was cleaned with the standard EUV cleaning recipe at AMTC. A STEAG Hamatech ASC 5500 instrument, using SPM/SC1 wet cleaning chemistry in conjunction with ultrasonic vibrations from a Megasonics tool was used for cleaning both the front and backsides of the mask. Finally, the cleaned *test* mask was used to expose resist-coated wafers on the MET and the results obtained were compared with those from a similar mask that was not contaminated and also did not undergo cleaning.

C. Analysis Results

Figure 1 shows the optical micrograph of the contaminated mask before cleaning. The contaminated fields are brown, while the uncontaminated fields are blank. Figure 2 shows the SEM images of line features in the contaminated and uncontaminated fields of the *test* mask before cleaning. The features in the contaminated fields are considerably larger than those in the uncontaminated fields, due to the build-up of the contaminants on top and on the sidewalls of the lines.

Figure 1: Optical micrograph of the *test* mask before it was cleaned.

Figure 2: SEM images of features in contaminated and uncontaminated fields of the *test* mask before cleaning.

Being a surface analysis technique with high spatial resolution, AES provides elemental information of the top, 2-5 nm of a surface. Figure 3 shows two Auger spectra of the

contaminated (red curve, on the bottom) and uncontaminated (blue curve, on top) fields of the contaminated mask before cleaning. The spectrum for the contaminated fields shows a clear Carbon peak at a binding energy of 272 eV, which has a higher intensity than the Carbon peak in the spectrum of the uncontaminated field. This suggests a larger amount of Carbon contamination in the exposed and thus contaminated field, which is also reflected in Carbon enrichment measured in a Carbon Auger map of the exposed area (see Figure 4). The spectra also show peaks corresponding to Cr, N, and O from the $Cr_xN_yO_z$ absorber material and Si and O of the Si capping layer, respectively, of the mask.

Figure 3: Auger spectra of the contaminated (red curve, on the bottom) and uncontaminated (blue curve, on the top) fields of the contaminated mask before cleaning.

Figure 4: Secondary electron image of the exposed field, showing the contamination as a dark area, which corresponds to the enrichment of the C KVV Auger signal (bright) at the right side.

III. Mask Patterning with MET

A. Procedure Description

The SEMATECH Berkeley MET installed at the Advanced Light Source synchrotron facility at Lawrence Berkeley National Laboratory currently uses spectrally pure, debris-free, undulator radiation as the source of the 13.5 nm EUV wavelength. The MET uses programmable coherence illumination[11] and provides imaging capabilities down to 12 nm, enabling advanced resist, mask, process, and metrology methods to be developed. Further details on the MET can be found elsewhere[12, 13]. The MET has a 0.3 numerical aperture (NA) and a 5× demagnification. The illumination conditions used were annular with an inner sigma of 0.35 and outer sigma of 0.55. The illumination angle of incidence is 4 degrees and parallel to the mask patterns. The resist images were recorded using a top-down SEM and analyzed offline with the software package SuMMIT[14]. In both cases, the photoresist was an 80 nm thick layer of EUVR-P1123. A focus and dose step sizes were 50 nm and 5%, respectively.

B. Results

Process window data for two sets of vertical lines and spaces were collected for each mask, one at a critical dimension (CD) of 40 nm and the other at a CD of 50 nm. For each set of data, process window, exposure latitude (EL) vs. depth of focus (DOF), and line edge roughness

(LER) were calculated. The result of the comparisons between the measured data for each mask is presented in Figs. 5 through 9.

The fitted Bossung curves obtained for the printed L/S patterns through-focus for each dose step are given in Figure 5. Each Bossung curve corresponds to a given exposure dose step. The iso-focal region of the fitted Bossungs generated for the printed L/S data fall at the expected CD in both the 40 nm and 50 nm cases. This is true for both the cleaned *test* mask [Figure 5 (a) and 5(b)] case as well as the *reference* mask [Figure 5(c) and Figure 5(d)].

The process windows calculated for the mask printed patterns at 50 nm CD and for 40 nm CD are given in Figure 6. There is reasonable agreement between the printed lines data for the two masks within error for both CDs of interest. Figure 7 shows a direct comparison of EL vs. DOF for the two masks. The observed changes in DOF are less than the focus step size, supporting the conclusion that there are no statistically appreciable printing differences between the two masks.

Figure 8 shows the LER measured for both mask patterns. In all four plots, the LER is found to be near 4 nm. The disparities seen in the two sets of data are not greater than what would be observed from multiple wafer printing with the same mask. Thus, it is safe to assume that the LER differences between the two masks are minimal, supporting the results observed from the CD process window performance.

Figure 5: Fitted Bossung curves obtained for the printed L/S patterns through-focus for the two masks. Each curve represents a dose step.

Figure 6: Process windows calculated from the printed L/S patterns for the two masks at 50 nm and 40 nm CDs.

Figure 7: Comparison of exposure latitudes calculated for the MET mask patterned line and space data at 50 nm and 40nm CD

Figure 8: Observed LER for the MET printed data at 40 nm and 50 nm CDs.

IV. Simulations

To verify the validity of comparing two different masks to evaluate the effect of mask cleaning, we performed rigorous aerial-image modeling. The relationship between mask structure

and lithographic performance with the EUV exposure tool was modeled using the EM-suite by Panoramic Technology[10]. The model accounts for all of the MET system parameters such as numerical aperture, illumination type, aberrations, and the angle of incidence for computing aerial images. Two sets of data, at line widths of 40 nm and 50 nm, are generated for each given mask structure modeled in 2D (xz plane) with a 40 multilayer stack on the substrate. Lithographic process analysis was completed on each data set to determine whether any substantial performance difference between the two masks could be seen.

Bossung curves were generated from the calculated aerial images through-focus (Figure 9). The exposure and focus values associated with each were chosen to match the experimental data. The skews in the traces are due to the MET pupil aberrations; the same was observed in the experimental data collected. The differences between the modeled data for the two masks at both 40 nm and 50 nm CD are minimal.

Figure 9: Bossung curves calculated through-focus from aerial image model simulations with E-M suite for the two different mask architectures. Each trace represents an exposure step that was chosen to match the experimental dose steps.

Figure 10 shows the corresponding process windows. Data for both mask structures at the two different CDs are shown. A point-spread function (PSF)-based resist model was used. The PSF was the HOST[15-17] function with a full width half maximum (FWHM) of 15 nm providing the best average fit to the experimental data. The modeled data for the two masks match well. The EL vs. DOF comparison of the two masks is shown in Figure 11. There is significant overlap in the calculated data, demonstrating that performance variations between the two masks are negligible.

Figure 10: Process windows generated by convolving calculated aerial images with resist blur function for both test and reference masks at the two different CDs.

Figure 11: Comparison of exposure latitudes calculated for the E-M Suite modeled aerial images. The modeled data of the two masks match very closely.

V. Discussion

The modeled data and analysis of the *test* and *reference* mask structures do not show any significant variation in lithographic performance, allowing the two mask types to be directly compared to evaluate the effect of mask cleaning. The SEMATECH Berkeley MET-printed L/S data for the contaminated and cleaned *test* mask was then compared to patterns from the new *reference* mask. The observed differences in the mask printing performance are shown to be trivial, leading to the conclusion that the cleaning process did not appreciably affect mask performance.

In addition to the mask comparison above, it is also interesting to directly compare the modeling and printing results to gain further insight into the accuracy of the models used. As stated previously, a simple 2D PSF model was used to represent the resist. Specifically, a 15 nm blur function was convolved with modeled aerial image intensities to best match the measured data in terms of process window performance. Measured and calculated EL, as shown in Figure 12, for the modeled data and for the MET printed patterns match fairly well. The notable differences in the data are near the zero DOF regions. The EL is higher for the simulated data in all of the cases considered. For both CDs in the case of the contaminated and cleaned TAR70 mask, the modeled EL is 32% higher than the patterned data. In contrast, the uncontaminated mask shows a 15% higher EL for the 50 nm lines and 32% higher EL for the 40 nm lines in the models. This discrepancy is attributed to the inability of the simple 2D resist modeling to accurately capture real-world resist thickness effects.

Although the results presented in this paper are encouraging, it is important to note that they do not yet provide enough information to be able to predict mask lifetimes in production environments. Mask lifetime is dictated by two items with the first being the contamination rate of the mask and the second being the number of allowable clean cycles. In this work we made no attempt to quantify contamination rates, since the studies were performed on the MET. In terms of the mask contamination rates, the MET would have extremely questionable correlation to a HVM exposure tool. Although not a fundamental limitation of a micro-exposure-tool based study, the present work also did not address the question of number of tolerable clean cycles. This important topic is currently under investigation and will be reported on in the near future.

Figure 12: Comparison of exposure latitudes calculated for the MET mask patterned data and for the E-M Suite modeled aerial images

Acknowledgments

We wish to acknowledge the expert support provided by Paul Denham, Brian Hoef, Gideon Jones, and Jerrin Chiu of the Center for X-Ray Optics at Lawrence Berkeley National Laboratory with the exposure tool as well as the entire CXRO engineering team for building and maintaining the EUV exposure tool. We acknowledge SEMATECH for the support of the SEMATECH Berkeley MET and in particular the programmatic support from Warren Montgomery, Bryan Rice, and Stefan Wurm. This work was supported in part by SEMATECH and carried out at Lawrence Berkeley National Laboratory's Advanced Light Source, which is supported by the DOE, Office of Science, and the Basic Energy Sciences under contract no. DE-AC02-05CH11231.

[1]R.H. Stulen and D.W. Sweeney, IEEE J. Quant. Elec. **35,** 694 (1999).

[2]*EUV Lithography*, edited by V. Bakshi (SPIE Press, Washington, 2007).

[3]O. Wood, C.-S. Koay, K. Petrillo, H. Mizuno, S. Raghunathan, J. Arnold, D. Horak, M. Burkhardt, G. McIntyre, Y. Deng, B. LaFontaine, U. Okoroanyanwu, A. Tchikoulaeva, T. Wallow, J. H.-C. Chen, M. Colburn, S. S.-C. Fan, B. S. Haran, and Y. Yin, Proc. SPIE **7271,** 727104 (2009).

[4]S. Wurm, F. Goodwin, and H. Yun, Next-generation lithography: *EUVL readiness for pilot line insertion*, Solid State Technology, 52(2), 2009. `http://www.solid-state.com/display_article/352195.`

[5]H. Kinoshita, T. Watanabe, A. Ozawa, and M. Niibe, Proc. SPIE **3412,** 358 (1998).

[6]B. LaFontaine, A. R. Pawloski, Y. Deng, C. Chovino, L. Dieu, O. R. Wood, II, and H. J. Levinson, Proc. SPIE **5374,** 300 (2004).

[7]A Wüest, *EUV Optics/Mask Contamination – Critical Issues Survey Results,* IEUVI Optics Contamination and Lifetime Technical Working Group Presentation, October 2, 2008. `http://ieuvi.org/TWG/ConOptics/2008/MTG100208/2-Wuest.pdf`

[8]Y.-J, Fan, L. Yankulin, G. Denbeaux, Y. Wang, R. Geer, A. Wüest, F. Goodwin, S. Huh, P. Naulleau, K. Goldberg, and I. Mochi, *Carbon contamination of Extreme Ultraviolet (EUV) Masks and its Effect on Imaging*, IEUVI Optics Contamination and Lifetime Technical Working Group Presentation, February 26, 2009. http://ieuvi.org/TWG/ConOptics/2009/MTG022609/2-Fan.pdf

[9]Y. Nishiyama, T. Anazawa, H. Oizumi, I. Nishiyama, O. Suga, K. Abe, S. Kagata, and A. Izumi, Proc. SPIE **6921,** 692116 (2008).

[10]Panoramic Technology, *EM-Suite: Core Lithography Simulation Package*, 2009. http://www.panoramictech.com.

[11]P. P. Naulleau, K. A. Goldberg, P. Batson, J. Bokor, P. Denham, and S. Rekawa, Appl. Opt. **42,** 820 (2003).

[12]P. P. Naulleau, Ch. N. Anderson, J. Chiu, K. Dean, P. Denham, K. A. Goldberg, B. Hoef, S. Huh, G. Jones, B. M. LaFontaine, A. Ma, D. Niakoula, J. Park, and T. Wallow, Proc. SPIE **6921,** 69213N (2008)

[13]P. P. Naulleau, K. A. Goldberg, E. Anderson, J. P. Cain, P. Denham, K. Jackson, A.-S. Morlens, S. Rekawa, and F. Salmassi, J. Vac. Sci. Technol. B **22**, 2962 (2004).

[14]SuMMIT Software Division of EUV Technology, *Summit Litho Image Analysis Software*, 2009. http://www.euvl.com/summit/.

[15]The HOST function (name coined by IBM) is derived from the reaction diffusion equations to provide the shape of the post exposure bake (PEB) deprotection blur (Lorentzian type widening of the features in resist) which occurs around each released acid. For the process window modeling, the HOST function is convolved with the aerial image to yield the deprotection statistics.

[16]F. Houle, W. Hinsberg, M. Morrison, M. Sanchez, G. Wallraff, C. Larson,and J. Hoffnagle, J. Vac. Sci. Technol. B 18, 1874 2000.

[17]Gregg M. Gallatin, Proc. SPIE 5754, 38 (2004)

List of Tables

Table 1: Contaminated/Cleaned TAR70 EUV mask (*test* mask)
Table 2: Uncontaminated LR-TaBN reference EUV mask (*reference* mask)

Table 1: **Contaminated/Cleaned TAR70 EUV mask (*test* mask)**

Structure	Material	n	k	Thickness (nm)
Absorber	Cr	0.93266	0.0387	70
Buffer	SiO_2	0.9781	0.0105	20
Capping Layer	Si	0.9991	0.0018	11
Multilayers	Mo/Si	0.9242/0.9991	0.0064/0.0018	N/A

Table 2: **Uncontaminated LR-TaBN reference EUV mask (*reference* mask)**

Structure	Material	n	k	Thickness (nm)
Absorber	TaBN[a]	0.9500	0.0289	55
Buffer	TaON[a]	0.9540	0.0260	15
Capping Layer	Ru	0.8869	0.0168	2.5
Multilayers	Mo/Si	0.9242/0.9991	0.0064/0.0018	N/A
Substrate	Quartz	0.9781	0.0105	N/A
Bias	1.5 nm	1.5 nm	1.5 nm	1.5 nm

[a]Rutherford backscattering spectrometry (RBS) measured values provided by supplier for specified thickness

List of Figures

Figure 1: Optical image of the contaminated mask before it was cleaned. 3
Figure 2: SEM images of features in contaminated and uncontaminated fields of the contaminated mask before cleaning. 3
Figure 3: Auger spectra of the contaminated (red curve) and uncontaminated (blue curve) fields of the contaminated mask before cleaning. 4
Figure 4: Secondary electron image of the exposed field, showing the contamination as dark area, which corresponds to the enrichment of the C KVV Auger signal (bright) at the right side. . 4
Figure 5: Fitted Bossung curves obtained for the printed L/S patterns through focus for the two masks. Each curve represents a dose step. 5
Figure 6: Process windows calculated from the printed L/S patterns for the two masks at 50 nm and 40 nm CDs. 5
Figure 7: Comparison of exposure latitudes calculated for the MET mask patterned line and space data at 50 nm and 40nm CD 5
Figure 8: Observed LER for the MET printed data at 40 nm and 50 nm CDs. 5
Figure 9: Bossung curves calculated through focus from aerial image model simulations with E-M suite for the two different mask architectures. Each individual trace represents an exposure step which was chosen to match the experimental dose steps. 6
Figure 10: Process windows generated by convolving calculated aerial images with resist blur function for both test and reference masks at the two different CDs. 6
Figure 11: Comparison of exposure latitudes calculated for the E-M Suite modeled aerial images. The modeled data are very closely matched between the two masks. 6
Figure 12: Comparison of exposure latitudes calculated for the MET mask patterned data and for the E-M Suite modeled aerial images 7

Captions to figures.

Lithographic performance evaluation of a contaminated EUV mask after cleaning

Figure 1: Optical image of the contaminated mask before it was cleaned.

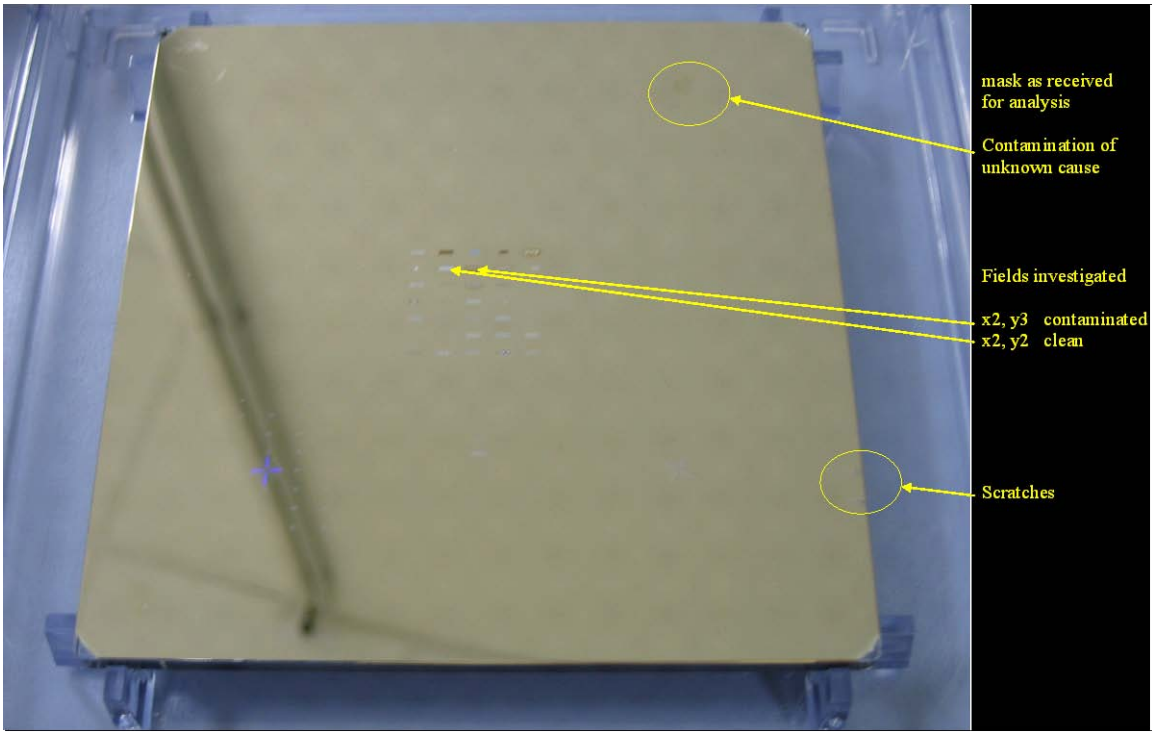

Figure 2: SEM images of features in contaminated and uncontaminated fields of the contaminated mask before cleaning.

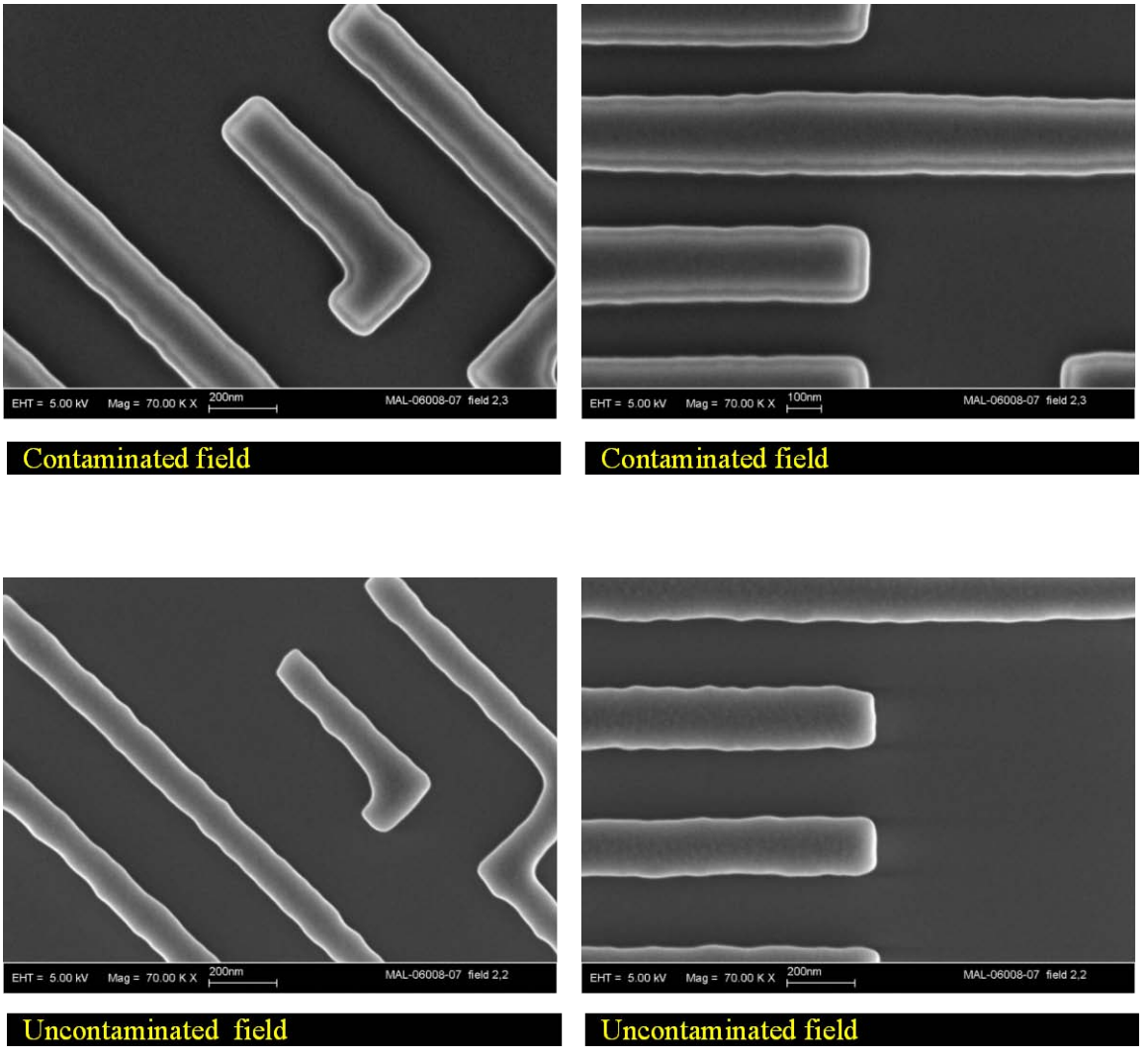

Figure 3: Auger survey spectra of the contaminated (red curve) and uncontaminated (blue curve) fields of the contaminated mask before cleaning.

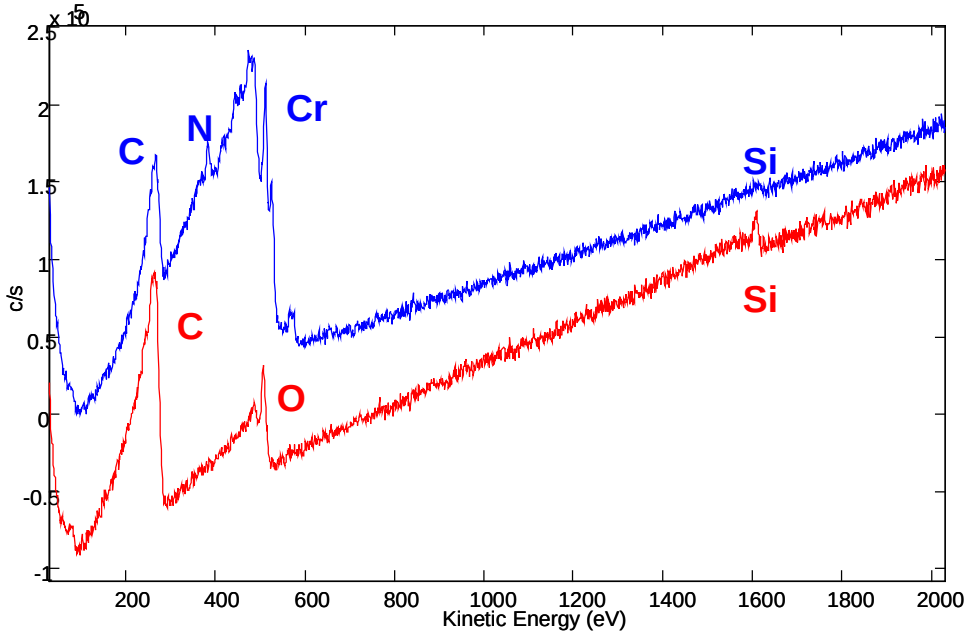

Figure 4: Secondary electron image of the exposed field, showing the contamination as dark area, which corresponds to the enrichment of the C KVV Auger signal (bright) at the right side.

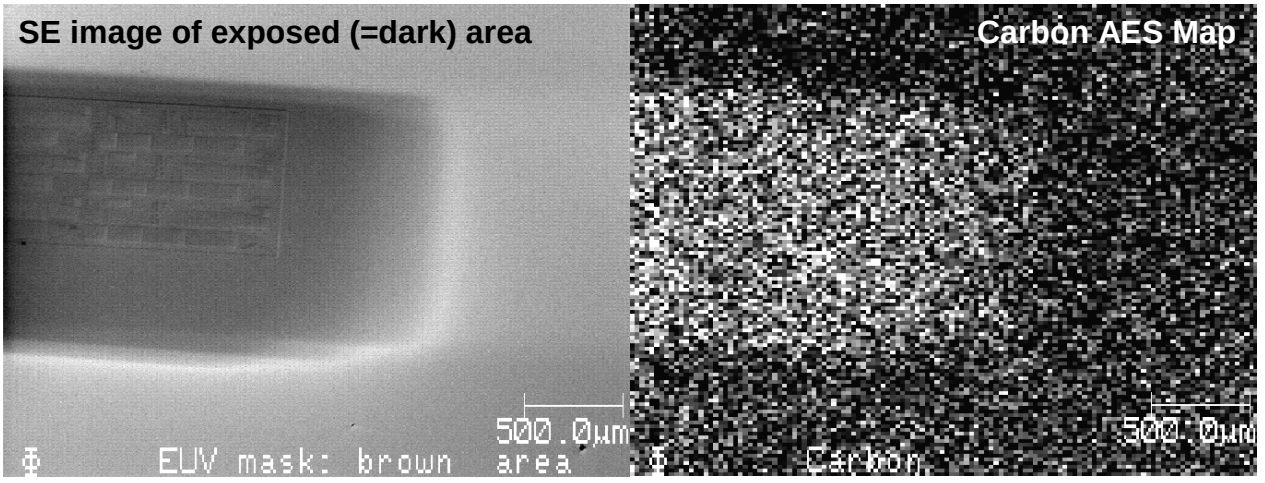

Figure 5: Fitted Bossung curves obtained for the printed L/S patterns through focus for the two masks. Each curve represent a dose step.

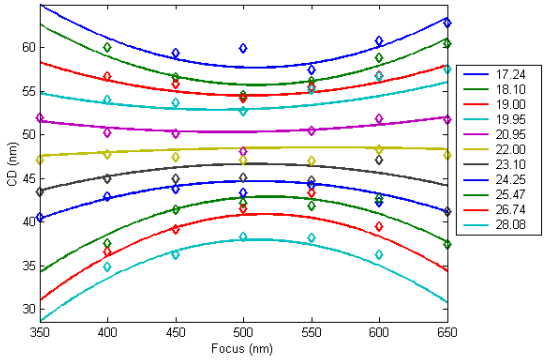

a) Cleaned mask, 50 nm L/S

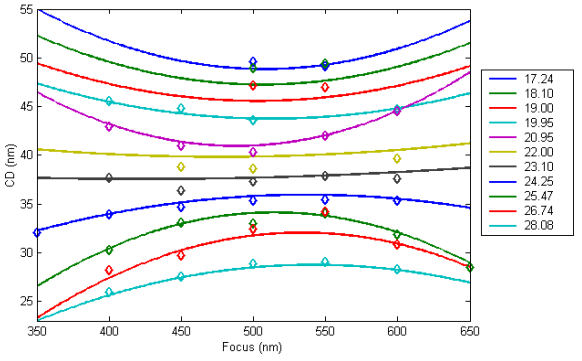

b) Cleaned mask, 40 nm L/S

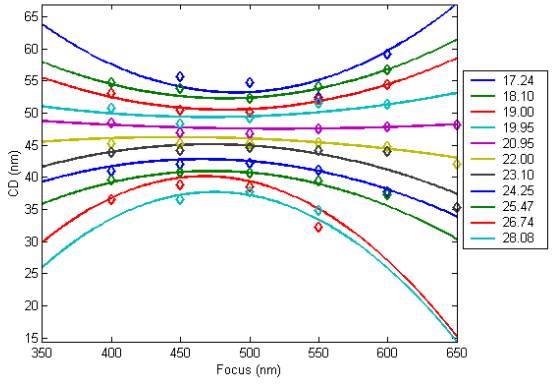

c) Reference mask, 50 nm L/S

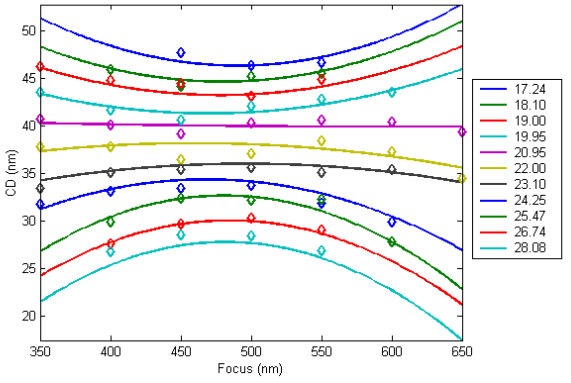

d) Reference mask, 40 nm L/S

Figure 6: Process windows calculated from the printed L/S patterns for the two masks at 50 nm and 40 nm CDs

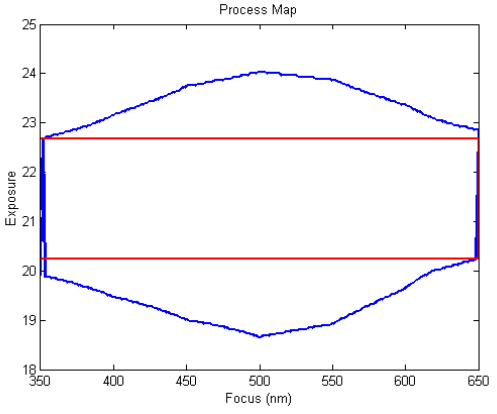

a) Cleaned mask, 50 nm L/S

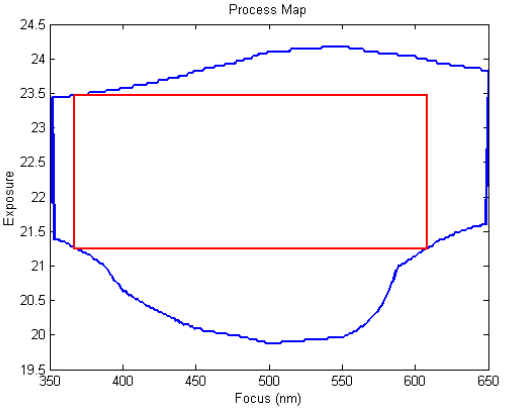

b) Cleaned mask, 40 nm L/S

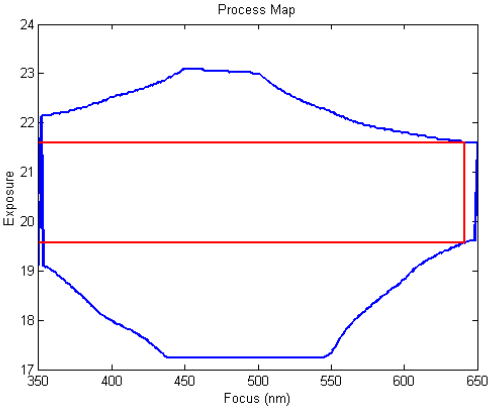

c) Reference mask, 50 nm L/S

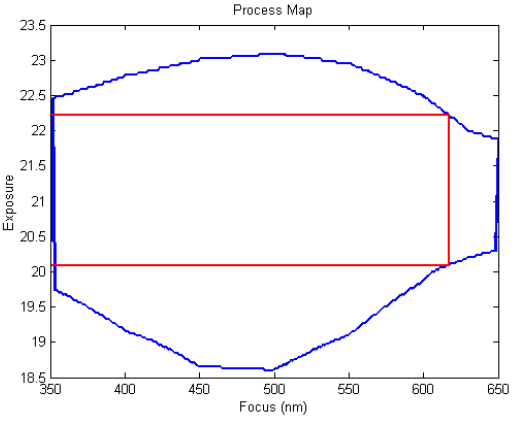

d) Reference mask, 40 nm L/S

Figure 7: Comparison of exposure latitudes calculated for the MET mask patterned line and space data at 50 nm and 40nm CD.

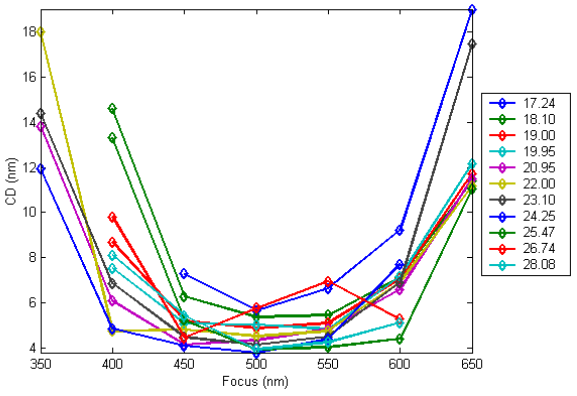

a) Cleaned mask, 50 nm L/S

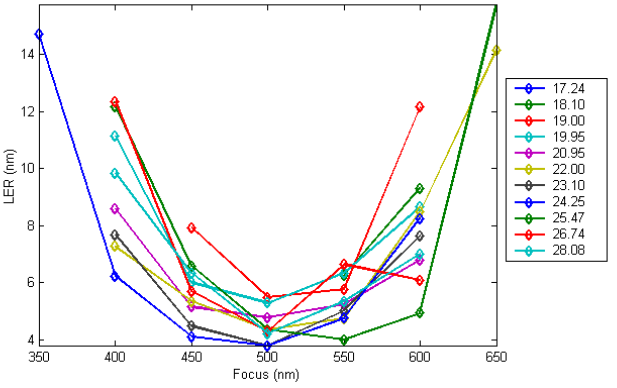

b) Cleaned mask, 40 nm L/S

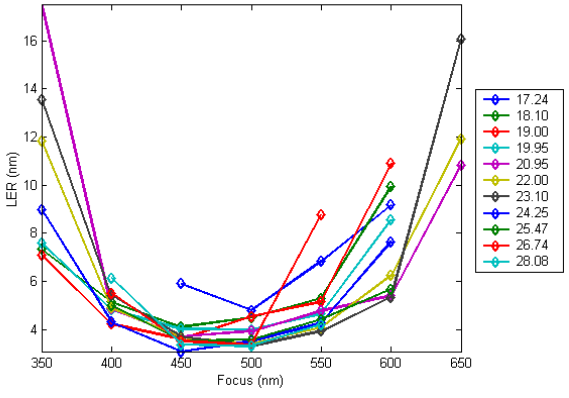

c) Reference mask, 50 nm L/S

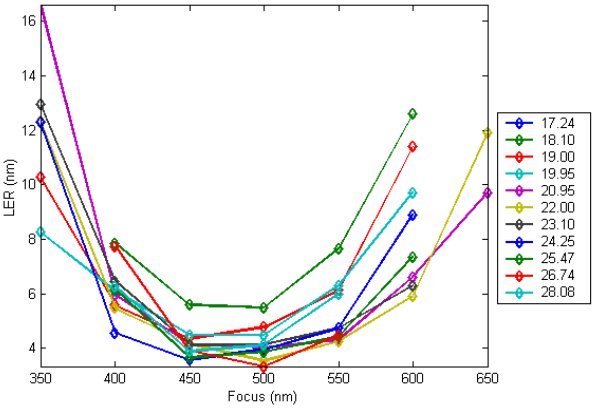

d) Reference mask, 40 nm L/S

Figure 8: Observed LER for the MET printed data at 40 nm and 50 nm CDs.

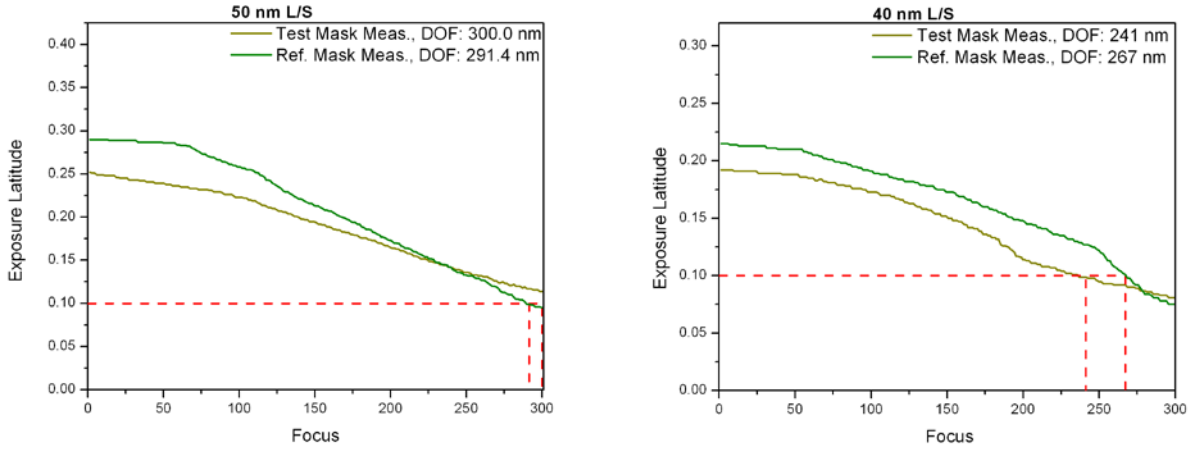

Figure 9: Bossung curves calculated through focus from aerial image model simulations with E-M suite for the two different mask architectures. Each individual trace represents an exposure step which was chosen to match the experimental dose steps.

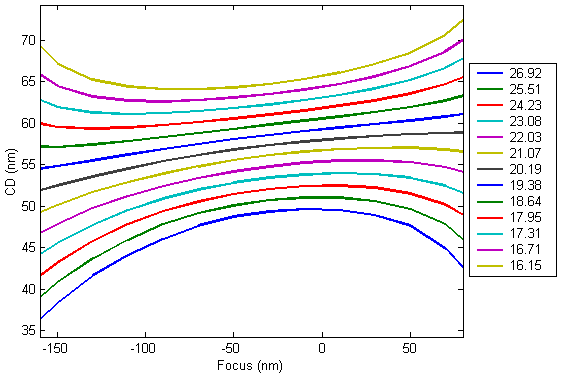

a) Cleaned mask, 50 nm L/S

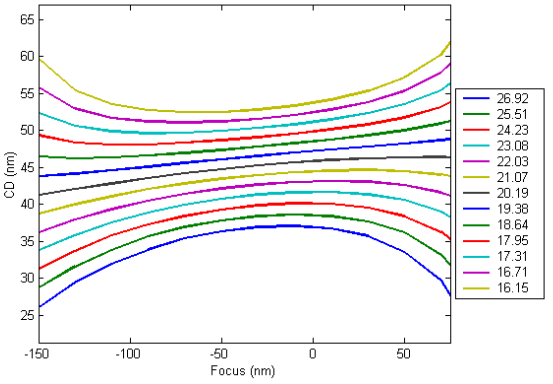

b) Cleaned mask, 40 nm L/S

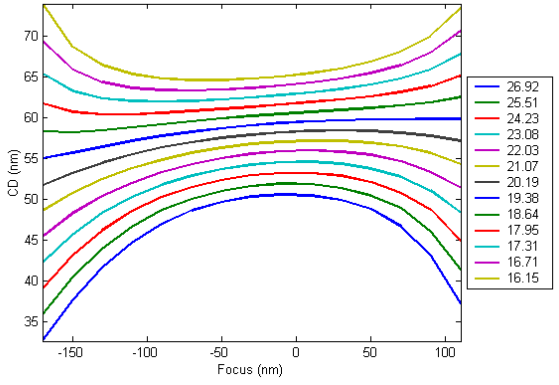

c) Reference mask, 50 nm L/S

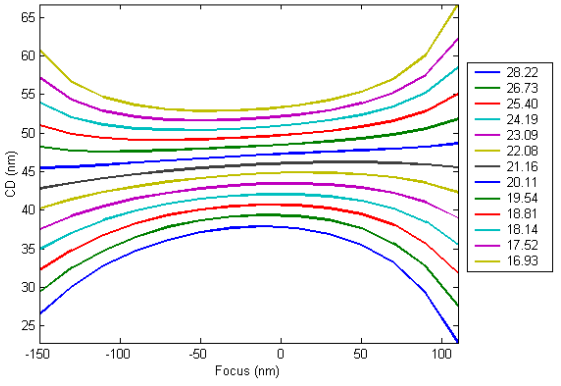

d) Reference mask, 40 nm L/S

Figure 10: Process windows generated by convolving calculated aerial images with resist blur function for both test and reference masks at the two different CDs.

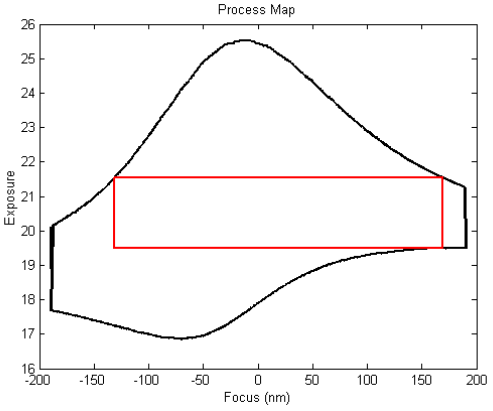

a) Cleaned mask, 50 nm L/S

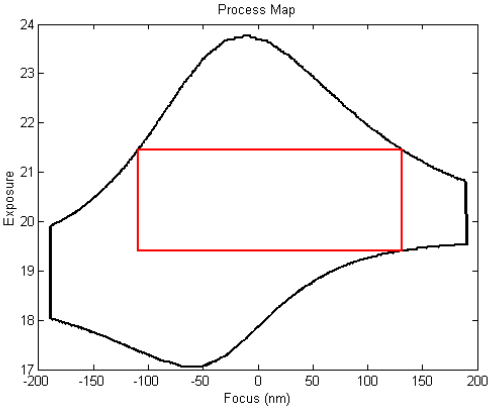

b) Cleaned mask, 40 nm L/S

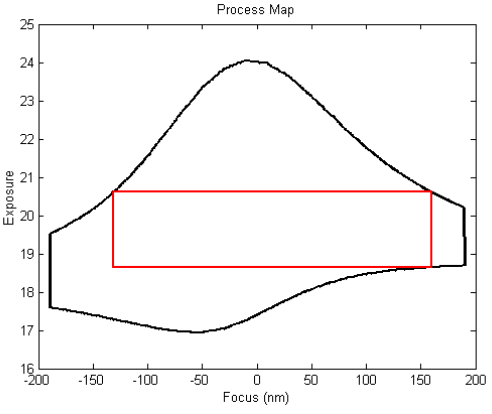

c) Reference mask, 50 nm L/S

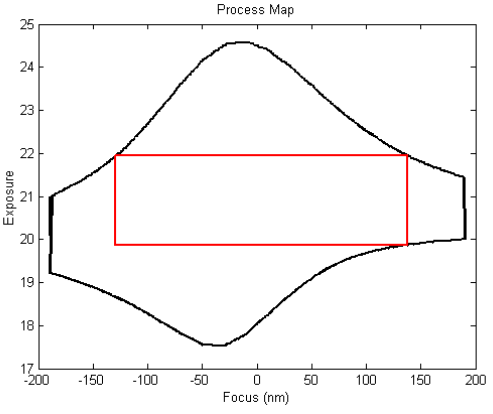

d) Reference mask, 40 nm L/S

Figure 11: Comparison of exposure latitudes calculated for the E-M Suite modeled aerial images. The modeled data are very closely matched between the two masks.

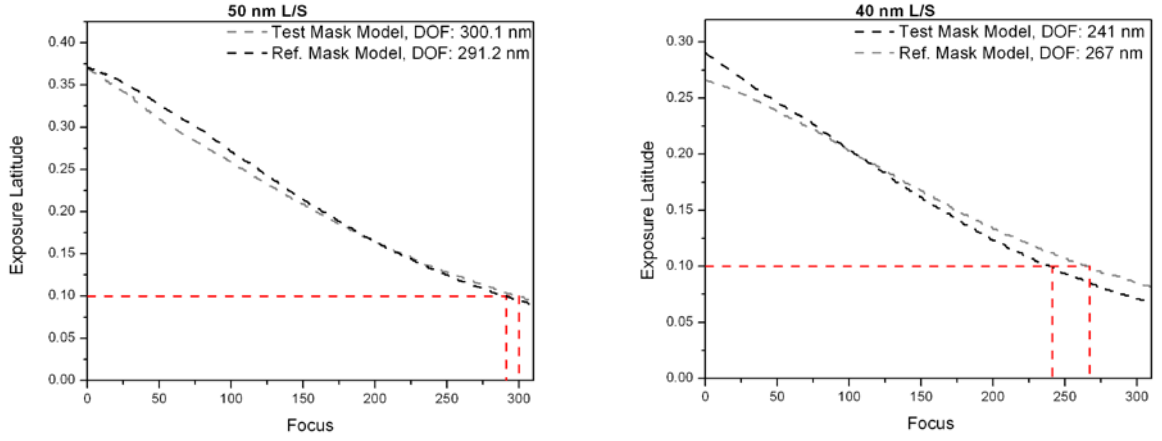
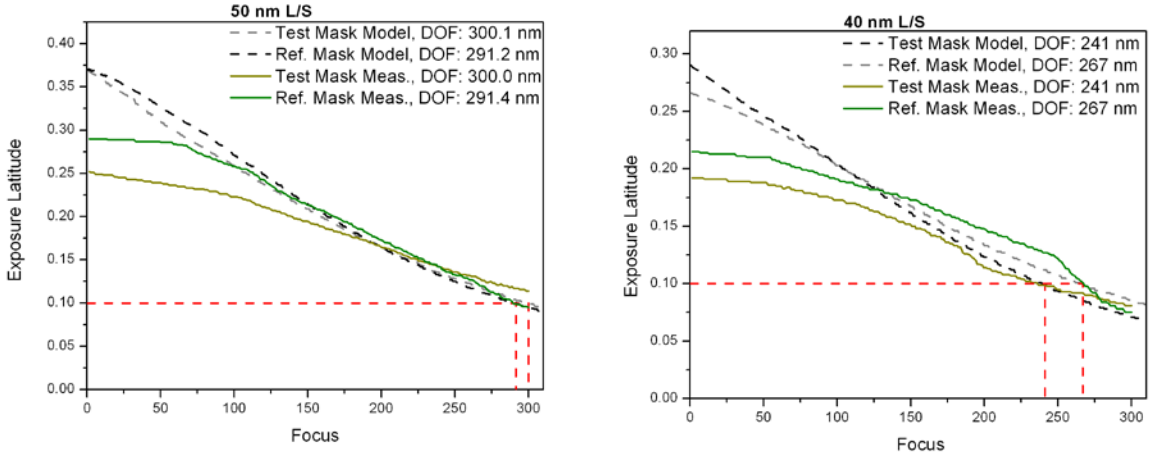
Figure 12: Comparison of exposure latitudes calculated for the MET mask patterned data and for the E-M Suite modeled aerial images**.**